Transportation Geotechnics 39 (2023) 100938

Contents lists available at ScienceDirect

Transportation Geotechnics

journal homepage: www.elsevier.com/locate/trgeo

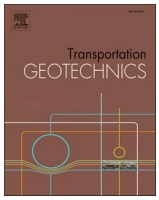

Numerical Evaluation of a Semi-Integral Bridge Abutment under Cyclic Thermal Movements

Pedro H.S. Silva [a], Yuri D.J. Costa [a,*], Jakob R. Walter [b], Behdad M. Kouchaki [c], Jorge G. Zornberg [c], Carina M.L. Costa [a]

[a] Department of Civil Engineering, Federal University of Rio Grande do Norte, Av. Sen. Salgado Filho, 3000, Natal, RN 59072-970, Brazil
[b] McMillen Jacobs Associates, 49 Stevenson Street Suite 1200, San Francisco, CA 94105, USA
[c] Department of Civil, Architectural and Environmental Engineering, The University of Texas at Austin, 301E. Dean Keeton St., Stop C1792, Austin, TX 78712, USA

ARTICLE INFO

Keywords:
Bridge abutment
Semi-integral bridge
Soil-structure interaction
Soil ratcheting
Cyclic loading

ABSTRACT

This paper presents a two-dimensional Finite Element (FE) simulation of the interaction between a semi-integral stub-type concrete bridge abutment and a granular backfill under cycles of temperature-induced lateral displacements. A numerical model was proposed utilizing an elastoplastic soil constitutive model considering the characteristics of a semi-integral bridge abutment located near the City of Palestine, Texas, USA. The numerical model was validated against data collected in the field from pressure cells installed on the soil side of the abutment of the semi-integral bridge. The long-term response of the backfill-abutment system representing a 50-year period was investigated numerically for annual cycles of expansion–contraction of the bridge. According to the results of the investigation, it is observed that annual cyclic lateral movements of the bridge abutment led to a rapid increase of lateral earth pressures upon the abutment wall. The locus of maximum lateral earth pressures occurred on the upper third of the abutment, which disagrees with the conventional earth pressure distributions often assumed in design guidelines for integral bridge abutments. The magnitude of the settlement trough that formed under annual cycles is deemed sufficient to negatively affect bridge performance soon after start of the bridge operation. Results predicted that cumulative shear strains prevailed in the region of the backfill soil far from the abutment wall. On the other hand, cumulative compressive volumetric strains (densification) dominated in the vicinity of the soil-abutment interface. While stabilization of lateral earth pressures on the soil-abutment interface was predicted to occur with the balance between both densification and shearing effects, settlements adjacent to the soil-abutment interface were predicted to persist as a consequence of the continued growth of cumulative shear strains (ratcheting) in the portion of the soil away from the abutment wall.

Introduction

Despite the acknowledged benefits and increasing application worldwide, the performance of integral and semi-integral bridges is not yet completely understood. The interaction mechanism of the backfill-abutment system that develops with the cyclic movements of the abutment remains a concern that requires further assessment. Although relatively small, the cyclic expansion and contraction of the bridge deck due to temperature fluctuations lead to the development of two important detrimental effects that may compromise the benefits of using integral and semi-integral bridges [13]: (1) the long-term build-up of lateral earth pressures on the abutment; and (2) the possibly significant deformations in the backfill behind the abutment. These effects can cause the backfill soil behind the abutment to develop lateral earth pressures that exceed those predicted by earth pressure theories and the ground surface to experience vertical displacements that may compromise the safety of road users and reduce roadway riding quality [7,14,2,3].

Several studies have been conducted to address the detrimental effects associated with integral bridge abutments. Some research programs have involved instrumentation of integral bridge abutments to monitor lateral earth pressure variations. Data collected from the field revealed that some abutments experienced an increase in the peak lateral earth pressure upon cycles of expansion–contraction of the bridge

* Corresponding author.
E-mail addresses: pedro.silva.064@ufrn.edu.br (P.H.S. Silva), yuri.costa@ufrn.br (Y.D.J. Costa), walter@mcmjac.com (J.R. Walter), mofarraj@utexas.edu (B.M. Kouchaki), zornberg@mail.utexas (J.G. Zornberg), carina.costa@ufrn.br (C.M.L. Costa).

https://doi.org/10.1016/j.trgeo.2023.100938
Received 24 September 2021; Received in revised form 3 October 2022; Accepted 16 January 2023
Available online 20 January 2023

[9,21,27,32], while other abutments showed an opposite behavior [32,16,27]. The discrepancies among earth pressure trends obtained with the data collected from these structures can be explained by the dependency of the earth pressures on many aspects that are distinctive to each site.

Another group of studies addressed the integral bridge backfill-abutment interaction problem by conducting numerical simulations and controlled experiments involving small-scale instrumented physical modeling [20,52,60,7,14,2,3]. Typical results show that lateral earth pressures acting on the wall as well as vertical displacements of the retained fill increase with increasing number of cycles. Settlements are found to occur near the moving wall interface while heaving is detected at a distance from the wall. The lateral earth pressures tend to stabilize after a number of cycles, while settlements at the backfill-abutment interface grow with no tendency toward stabilization. One of the reasons for the observed typical results have been explained by an accumulation of irreversible strains in the backfill, a phenomenon known as ratcheting [20,52,26,60].

Although progress has been made on understanding the response of the backfill-abutment system with cyclic movements of the abutment induced by temperature fluctuations for the case of integral bridges, little attention has been paid to the behavior of semi-integral bridge abutments. The discrepancy between the data availability for integral bridges as compared to semi-integral bridges is evident, in spite of the growing popularity of semi-integral bridges in the past few decades [13,37].

Semi-integral bridge abutments have been reported to present some advantages over integral bridge abutments. For example, piles supporting an integral bridge abutment can experience flexural stresses considerably larger than those of their jointed bridge counterparts [13].

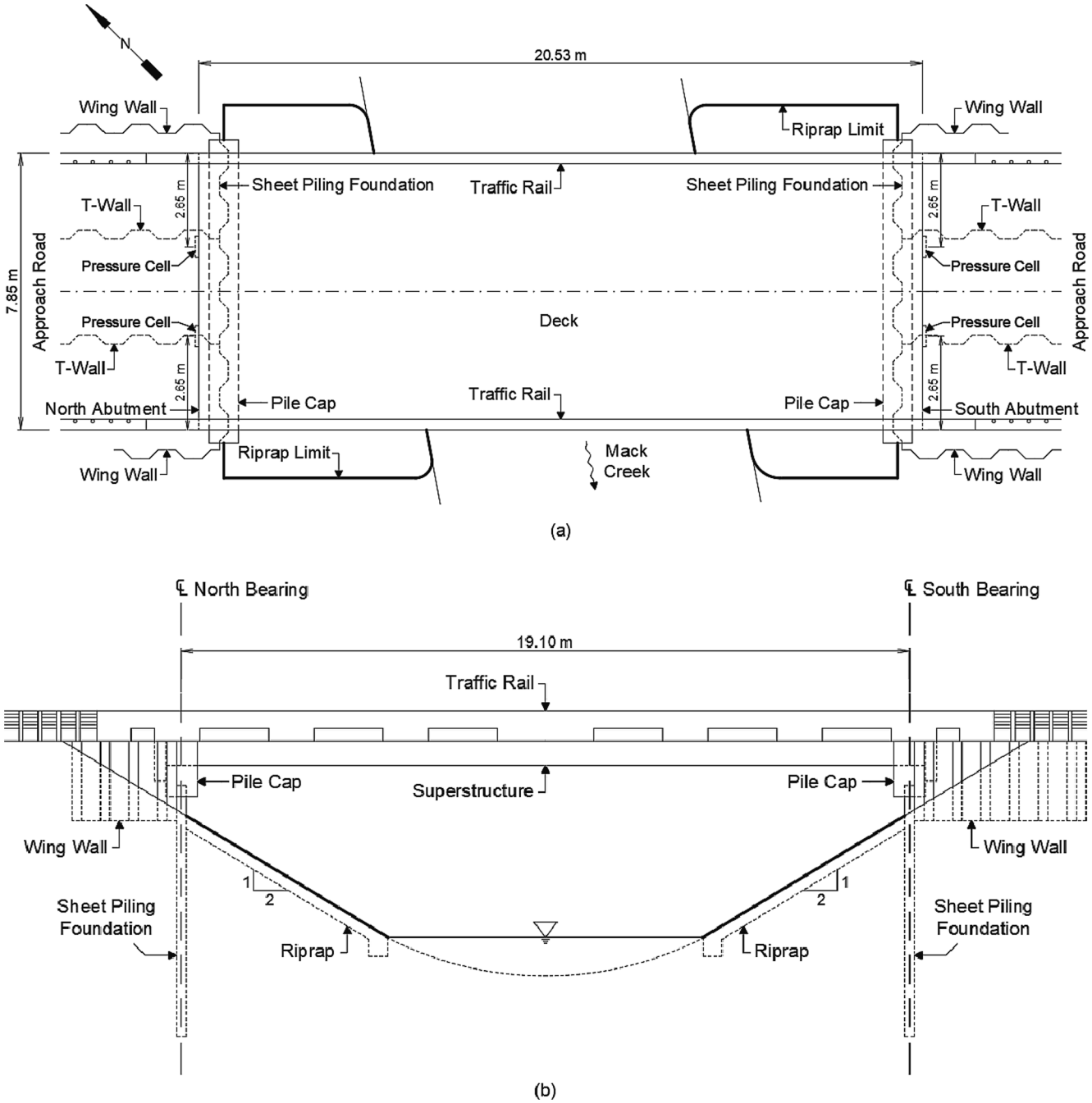

Fig. 1. Schematic views of the bridge: (a) plan view; (b) elevation view.

High flexural stress levels can reduce the pile resistance to bending and lead to formation of plastic hinges in the pile shaft. Conversely, the superstructure of a semi-integral bridge can move in the longitudinal direction independent of the underlying foundation structure, thus reducing stresses and bending moments in the supporting piles as well as tolerating the number of cycles expected during the bridge lifespan without any damage [6].

Despite the advantages and increasing usage of semi-integral bridges in engineering practice, the limited number of investigations with semi-integral bridge abutments may have compromised a broader acceptance. The lack of consistency among design guidelines and construction practices of semi-integral bridge abutments may be a consequence of the limited number of studies on these structures [4,13,15].

Accordingly, this study presents a two-dimensional FE analysis on the interaction between a semi-integral stub-type concrete bridge abutment and the retained backfill under cycles of lateral displacements due to temperature fluctuations. The long-term response of the backfill-abutment system was investigated for annual cycles of expansion–contraction of the bridge. The developed numerical model was validated against data collected in the field from earth pressure cells installed on the retained soil side of a semi-integral bridge abutment. Emphasis is placed on examining the lateral earth pressures on the abutment and deformations in the backfill soil throughout cycling.

Characteristics of the monitored semi-integral bridge

Bridge location and description

The semi-integral bridge evaluated in this study is located where the Anderson County Road 2133 crosses Mack Creek, near the City of Palestine, Texas, USA. Fig. 1 shows schematic views of the bridge and Fig. 2 presents a detail of the semi-integral bridge system in the region of the abutment. The structure is a stub-type semi-integral abutment bridge with a length of 20.53 m and a width of 7.85 m. It involves a single span with a bearing-to-bearing length of 19.10 m. The superstructure consists of a 0.15-m thick reinforced concrete deck supported on 0.5-m high prestressed concrete box beams. The superstructure is integrally connected to 1.05-m high and 0.3-m thick reinforced concrete abutments.

The bridge abutments are supported by 6.6-m long driven steel sheet piles connected to 0.83-m wide and 0.75-m high reinforced concrete pile caps. A laminated elastomeric bearing pad (LEBP), with a thickness of 70 mm, was placed between the pile cap and the bridge superstructure, and a preformed bituminous fiber material (PBFM), with a thickness of 40 mm, was placed between the pile cap and the bridge abutment. The bridge wingwalls were constructed normal to the abutments and are composed of 2.1-m long driven steel sheet piles. Two additional walls, built with steel sheet piles measuring 1.5 m in length, were installed between the wingwalls and were connected to the foundation piling. These two additional walls are identified in Fig. 1(a) as "*T*-walls". All sheet piles composing the foundations, wing walls and *T*-walls were built with PZC-18 profiles manufactured by Gerdau [24].

Subsoil and backfill characteristics

A subsurface characterization was conducted at the bridge site, which included Texas Cone Penetrometer (TCP) tests carried out near each abutment [59]. The procedure followed in the TCP tests is described in TxDOT Designation: Tex-132-E – Test Procedure for Texas Cone Penetration [55]. Information about the subsoil profile at the north abutment site is provided in Table 1.

The backfill in contact with the abutment is a free-draining material composed of industrially produced gravel particles from large pieces of crushed rock. The aggregate is composed of 88 % gravel particles with

Table 1
Subsoil profile and TCP test results [59].

Number of blows/penetration in mm	Depth[(1)] (m)	Subsoil profile
–	0.0	Silty sand (0 to −6.5 m) GWT:
–	–2.0[(2)]	−4.85 *m*
22/300	–3.5	
15/300	–5.0	
17/300	–6.5	
84/300	–8.0	Sandy clay
100/187.5	–9.5	
100/187.5	–11.0	
100/62.5	–12.5	
100/50	–14.0	
100/62.5	–15.5	

Note: [(1)]depth below approach road level; [(2)] test start depth.

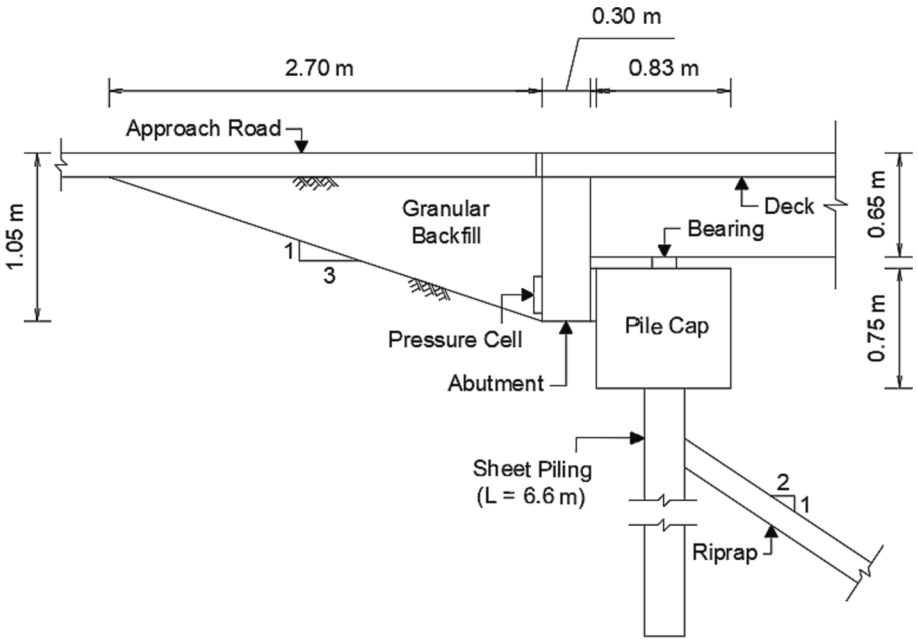

Fig. 2. Cross-section of the semi-integral bridge system elements near the abutment.

an average particle size of 4.7 mm and a specific gravity of 2.66. Its coefficient of uniformity is 3.47 and its coefficient of curvature is 1.24. According to the Unified Soil Classification System (USCS), the material classifies as a clean, poorly graded gravel (GP).

A series of conventional consolidated isotropically drained (CID) triaxial tests were conducted to estimate the parameters of the backfill material. Since the backfill particles can be as big as 13 mm, a 152-mm diameter triaxial cell was assembled to accommodate the testing program. Three tests at effective confining pressures of 41 kPa, 62 kPa, and 83 kPa were carried out with specimens prepared with a target relative density (D_r) of 50 % (Eq. (1)). Shear strength and volume change properties of the backfill material are summarized in Table 2.

$$D_r(\%) = \frac{e_{max} - e}{e_{max} - e_{min}} \times 100 \quad (1)$$

Where: e = void ratio; e_{max} = void ratio in loosest state; e_{min}= void ratio in densest state.

Field instrumentation and monitoring

Lateral earth pressures on the abutments were monitored in the field by vibrating wire (VW) contact pressure cells, model 4810, manufactured by Geokon [23]. Two pressure cells were installed vertically against each abutment wall face prior to backfilling, at a depth of 1 m below the abutment top. After installing on the abutment faces, protective pouches of geotextile filled with fine sand were placed around the pressure cells to prevent point loading by the crushed rock backfill. The locations of the pressure cells are schematically shown in Fig. 1(a) and 2. Dataloggers with temperature sensors were installed under the bridge deck to record the ambient air temperature and pressure cell readings on an hourly basis.

Temperature values provided by the temperature sensors were compared to the data of ambient air temperature collected by a weather station at the City of Palestine, Texas. Congruence between the temperature values collected by both the weather station and the temperature sensors was observed, which indicates that the temperatures recorded by the dataloggers were representative of the site ambient air temperature. Since similar temperature readings were collected from both temperature sensors below the bridge, the ambient air temperature adopted for this study corresponds to the average between the readings from both sensors. Similarly, the lateral earth pressure adopted for this study was the average between readings from the two pressure cells placed at each abutment. Further details about the instrumentation and monitoring of the bridge in the field is provided by Walter [57].

Characteristics of the numerical simulations

Constitutive models and material properties

The behavior of the soil materials was represented by the Hardening Soil (HS) constitutive model, developed under the framework of the theory of plasticity, in which a stress–strain relationship, due to primary loading, is assumed to be hyperbolic [49]. The HS model adopts a Mohr-Coulomb failure criterion, which was defined considering undrained conditions for the sandy clay layer and drained conditions for the silty sand layer and the gravel backfill. The material properties adopted for the soils are listed in Table 3. Unsaturated features of soil behavior were not considered in the present analysis. Also, although alternating cycles of wetting and drying can also lead to settlements and collapse of soils, this behavior was not considered in the current study.

Parameters assigned for the backfill gravel were adopted using the results from the previously described laboratory tests. Parameters for the silty sand and the sandy clay layers were defined based on the available TCP test results and relevant correlations [25,34,39,50,53,54,56]. Specifically, the undrained shear strength for the sandy clay layer was estimated as 2.15 N_{TCP} (kPa), as suggested by Vipulanandan et al. [56], and the effective friction angle for the silty sand layer was estimated from correlations reported in TxDOT [54]. The parameters for soil stiffness were assigned for a reference confining pressure of 100 kPa. The reference tangent stiffness for primary oedometer loading was assumed to equal the reference drained Young's modulus at 50 % of maximum strength (E_{50}^{ref}), as per Obrzud and Truty [43]. The reference Young's modulus for unloading/reloading was set to 3 E_{50}^{ref}, which is the recommended default setting used in Plaxis 2D [10].

The power coefficient for the stress-level dependency of stiffness (m) was adopted as 0.5 for the soil materials [30,18,48]. The Poisson's ratio for unloading/reloading (ν_{ur}) was set to 0.2, which is the default setting used in Plaxis 2D [10].

Table 4 lists the parameters of the structural elements adopted for the simulations. The material structural properties correspond to those of the bridge evaluated in this study [1,24,36,44,51,59]. The stress–strain behavior of the structural materials was represented using an isotropic linear-elastic relationship.

An important parameter governing the soil-structure interface properties in the software Plaxis 2D is the strength reduction factor (R_{inter}) [10]. R_{inter} is the ratio between interface friction coefficient (μ_{inter} = tan δ) and soil friction coefficient (μ = tan ϕ) or the ratio between interface cohesion ($c_{\ inter}$) and soil cohesion (c), and varies between 0 and 1. In the present study, R_{inter} values used for soil-structure interaction were 0.5 for the soil-steel interface and 0.7 for the soil-concrete interface [42,10,41]. A virtual thickness factor of 0.1, which is the default value of the software [10], was applied to the interface boundaries.

A sensitivity analysis was conducted to assess the influence of the adopted strength reduction factor (R_{inter}) for the abutment-backfill interface on the numerical model response. Values of R_{inter} ranging from 0.1 to 0.9 were evaluated and the corresponding results were compared to R_{inter} = 0.7, which is the baseline value usen in this study. It was found that the assumption of R_{inter} = 0.7 led to the most suitable predictions of lateral earth pressures.

Table 2
Summary of triaxial test results with backfill material.

$\sigma_3^{'}$(kPa)	$\phi_p^{'}$(°)	ψ (°)	$(-d\varepsilon_v/d\varepsilon_1)_{max}$
41	48.0	10.6	0.449
62	45.0	7.1	0.284
83	42.5	3.9	0.147

Note: $\sigma_3^{'}$ = effective confining pressure; $\phi_p^{'}$= peak friction angle; ψ = dilatancy angle; $(-d\varepsilon_v/d\varepsilon_1)_{max}$ = maximum strain increment ratio.

Table 3
Soil properties adopted in the numerical model.

Parameter	Soil material		
	Sandy clay	Silty sand	Gravel
Unit weight, γ (kN/m^3)	19	17	20
Saturated unit weight, γ_{sat} (kN/m^3)	22	20	23
Drained Young's modulus at 50 % of max. strength, E_{50}^{ref}(MPa)	60	40	30
Tangent stiffness for primary oedometer loading, E_{oed}^{ref} (MPa)	60	40	30
Young's modulus for unloading/reloading, E_{ur}^{ref}(MPa)	180	120	90
Poisson's ratio for unloading/reloading,ν_{ur}	0.2	0.2	0.2
Undrained shear strength, S_u(kPa)	210	–	–
Effective cohesion, $c^{'}$(kPa)	–	15	1
Peak friction angle, $\phi_p^{'}$(°)	–	31.5	43
Dilatancy angle, ψ (°)	0	0	10

Table 4
Structural material properties used in the numerical model.

Parameter	Material Reinforced concrete	PBFM	Sheet pile
Unit weight, γ (kN/m^3)	25	10	–
Young's modulus, E (GPa)	30	4	–
Poisson's ratio,ν	0.2	0.2	0.3
Axial stiffness, EA (kN/m)	–	–	3.16×10^6
Flexural stiffness, EI (kNm^2/m)	–	–	7.33×10^4
Weight per unit length, w (kN/m/m)	–	–	1.16

Note: A = cross-section area of sheet pile;I = moment of inertia of sheet pile.

FE model

A plane-strain FE model (Fig. 3) was developed for the north abutment of the bridge using the software Plaxis 2D version 2016 developed by Plaxis BV [10]. The model boundaries extended to a length of 40 m in the horizontal direction and 20 m in the vertical direction. These dimensions were assumed to be sufficiently large to minimize boundary effects [33,46]. The lateral boundaries of the mesh are free to move in the vertical direction and fixed in the horizontal direction. The base of the soil model is constrained from moving in both vertical and horizontal directions. A mesh with 4,410 15-node triangular solid elements was used in the simulations. A refined mesh was adopted in the backfill-abutment zone, which involved a comparatively high number of elements in the soil-abutment loading zone.

The soil materials (i.e., the gravel backfill, the silty sand layer and the sandy clay layer), the reinforced concrete and the PBFM were modeled using 15-node triangular elements. The foundation sheet piling was modeled by plate elements with the same axial and flexural stiffnesses of the sheet piles used for bridge construction. The *T*-wall sheet piling was modeled by fixed-end anchor elements with a vertical spacing of 150 mm and a horizontal length of 7 m. The vertical spacing of the anchor elements was defined by discretizing the height of the *T*-walls in ten equal parts, while the horizontal length of the anchor elements was assumed as the average length of the *T*-walls. The anchor axial stiffness adopted in the numerical analysis was 2.99×10^6 kN. The effect of the bridge superstructure on the abutment and pile cap was represented by static equivalent loads. Accordingly, the superstructure-abutment system was simulated as a bi-supported beam subjected to distributed loading due to the structure's self-weight.

The effects of expansion and contraction of the bridge superstructure on the abutment due to temperature changes were simulated by imposing prescribed horizontal displacements at the top of the abutment [8,40,7,14,3]. The effect of the approach road on the underlying soil was represented by a surface pressure of 3 kPa, which was estimated considering the characteristics of the subbase and paving materials [59].

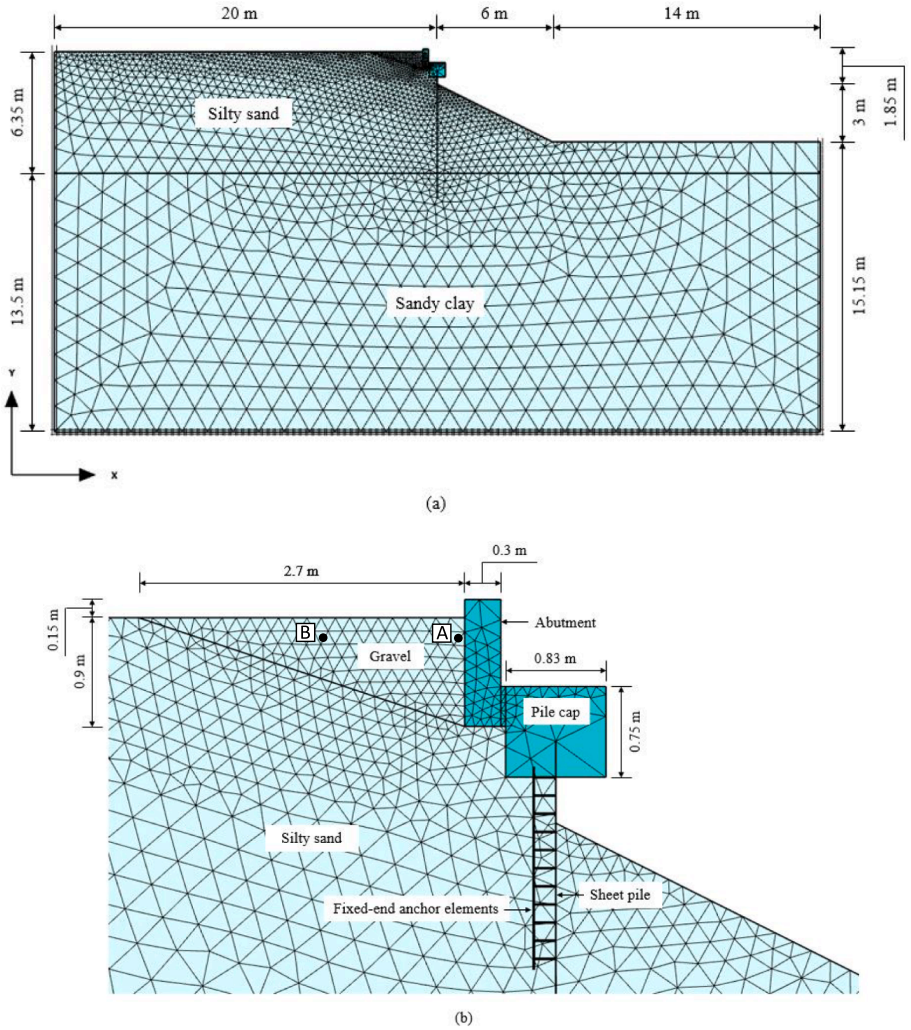

Fig. 3. FE model of the semi-integral bridge: (a) full model; (b) detail near the abutment.

Imposed lateral displacements

The bridge length changes (ΔL) due to temperature variation was predicted according to [1]:

$$\Delta L = \alpha \bullet L \bullet \Delta T \quad (2)$$

where α is the thermal expansion coefficient of the bridge material, L is the bridge length, and ΔT is the bridge temperature variation. In the absence of laboratory tests, a coefficient of thermal expansion $\alpha = 10.8 \times 10^{-6}$ /°C was assumed for the concrete, which is within the range recommended by AASHTO [1]. The prescribed horizontal displacements were calculated by dividing the ΔL value predicted using Eq. (2) by two. This assumption was adopted for the numerical simulations conducted in this study since both north and south backfills were built with the same material. A similar approach was used by other investigations [15,8,7,31].

Due to limited field instrumentation and to simplify the complex interaction mechanisms of heat transfer and flow involving the bridge and the surrounding environment [19,28,35], daily bridge temperature variations were assumed to equal the daily ambient air temperature variations. The daily change in temperature (ΔT) in Eq. (2) was defined as the difference between the maximum temperature (T_{max}) and the minimum temperature (T_{min}) recorded by the temperature sensors installed below the bridge deck within a 12-hour interval. The prescribed horizontal displacements (d) of the abutment acting against the backfill were then estimated as the difference between T_{min} and T_{max} in each day, while the prescribed horizontal displacements pulling the abutment away from the backfill were estimated as the difference between T_{max} of each day and T_{min} of the subsequent day. This approach led to daily cycles with variable horizontal displacements (d). In the daily cyclic movements, the abutment leaves the vertical (neutral) position (O) toward the extreme passive position (P), then moves to the extreme active position (A) passing though the neutral position (O) and finally returns to the neutral position (—— O-P-O-A-O mode).

Under annual cycles, the bridge length variation (ΔL) was predicted by assuming a temperature amplitude $\Delta T = 45$ °C in Eq. (2), following AASHTO's [1] recommendation for the location of the bridge. This resulted in annual cycles with imposed horizontal displacements (d) of $\pm$ 5 mm. Since bridge construction was completed in the summer, the bridge initially contracted until the winter, when the minimum longitudinal length was reached. Then, the bridge expanded until the summer of the next year and concluded the annual cycle. To represent this sequence, the numerical simulations were conducted with the abutment initially displacing away from the backfill and then moving towards the backfill (O-A-O mode). A total of 50 cycles of prescribed horizontal displacements of the abutment were used to simulate the effect of a 50-year period on the bridge.

The phases considered in the numerical simulations included: (1) calculation of the initial geostatic stresses in the subsoil; (2) installation of the structural elements (sheet piles, anchors, pile cap, abutment and PBFM), placement of the granular backfill and application of the loads on the abutment, pile cap and backfill; and (3) application of sequential prescribed horizontal displacements at the top of the abutment. The lateral displacements at the top of the abutment in the daily and annual cycles were imposed in ten increments (i.e., five increments in active movement and five increments in passive movement).

Validation of the numerical model

The numerical model was validated by comparing predicted lateral earth pressures against field data collected from the pressure cells installed on the Mack Creek semi-integral bridge abutment. To facilitate computational efficiency, calculations were restricted to a 100-day period, beginning at the start of field monitoring. The numerical simulation involved applying prescribed daily horizontal displacements (d) to the abutment top to represent the temperature-induced, cyclic lateral displacements of the abutment due to daily maximum expansions and contractions of the bridge.

Fig. 4 shows the daily horizontal displacements estimated using the previously described approach. A positive sign corresponds to a displacement d when the abutment moves toward the retained backfill (passive movement). Most estimated horizontal displacements fall within a range of $\pm$ 1.5 mm, which corresponds to a normalized displacement d/h of $\pm$ 0.17 % (where h is the abutment height in contact with the backfill).

The maximum and minimum daily cyclic lateral earth pressures, as obtained from field measurements, were compared against the numerical predictions in a 1:1 scatter plot (Fig. 5). Each value from the numerical simulation is the average horizontal stress from 11 stress points on the backfill-abutment interface, which correspond to the elevation of the pressure cells in the Mack Creek abutment. The relationship between numerical predictions and field measurements yielded a Pearson's product-moment correlation coefficient (r) of 0.905, which corresponds to a determination coefficient (r^2) of 0.82. A Pearson's coefficient r of 0.905 indicates a very strong correlation between numerical predictions and field measurements [47].

Considering the results discussed previously, the response of the numerical model is deemed to closely predict the field monitoring data, with very small discrepancies between them. Hence, the proposed FE modeling and adopted procedures are deemed adequate for the subsequent parametric evaluation on the long-term performance of a semi-integral bridge.

Results

Lateral earth pressures on the abutment wall

The peak lateral earth pressures predicted for each cycle as a function of the abutment height ratio for selected annual cycles is shown in Fig. 6. The abutment height ratio corresponds to the elevation from the abutment toe, z, normalized against the height of the abutment in contact with the backfill, h. The peak lateral earth pressures represent the values obtained when the abutment wall reaches the maximum annual passive movement. For reference, predicted pressure distributions corresponding to at-rest, active and passive conditions are also plotted in Fig. 6. Active and passive conditions were defined according to Rankine's theory [45], while the at-rest condition was predicted according to Jaky [29]. The results in Fig. 6 also show the lateral earth pressures predicted using the design methods specified in document PD 6694–1 [12] and in the Massachusetts Department of Transportation's Bridge Design Guidelines [38]. Both methods were formulated for integral bridge

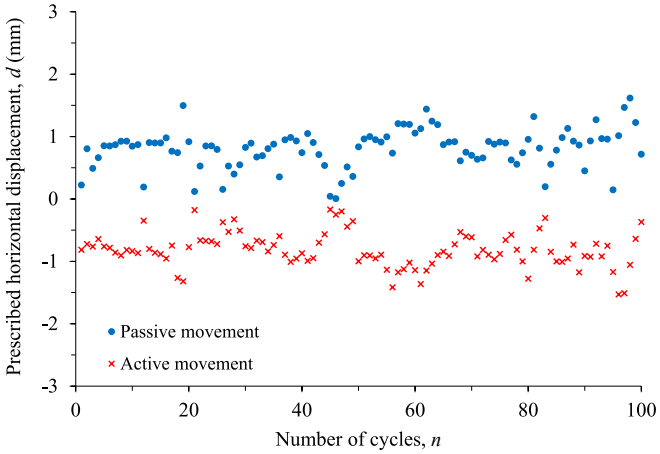

Fig. 4. Estimated daily horizontal displacements.

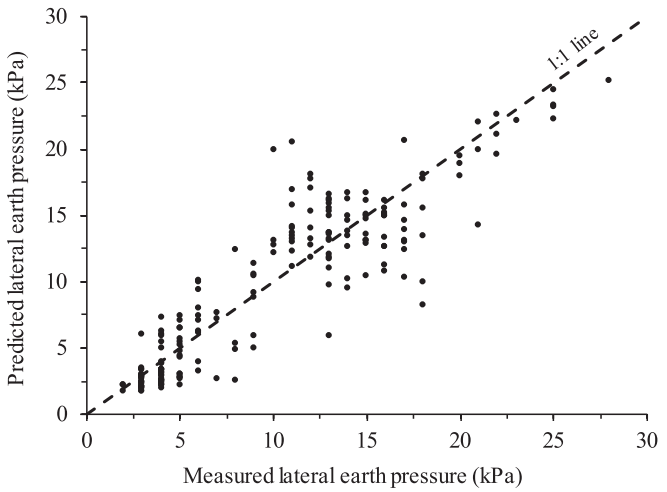

Fig. 5. Measured *versus* predicted lateral earth pressures in a 1:1 scatter plot.

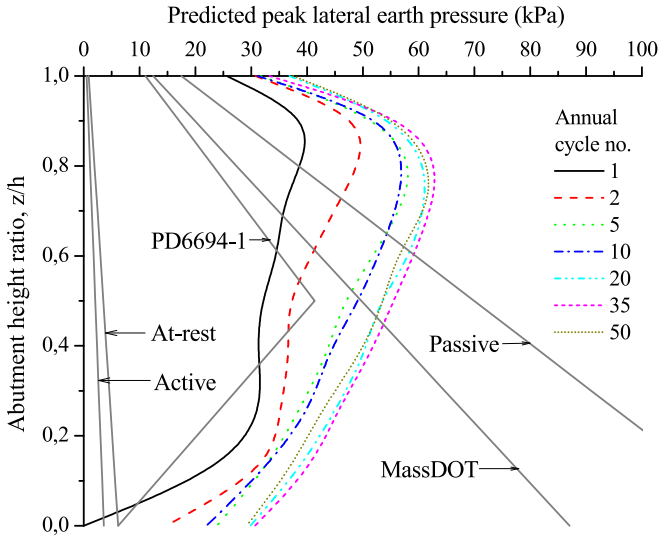

Fig. 6. Predicted lateral earth pressure distributions along abutment height for select annual cycles and comparison with distributions from design guidelines.

abutment.

The method described in PD 6694–1 [12] assumes the use of an earth pressure coefficient, K^*, over the upper half of the abutment, obtained from Eq. (3). The earth pressure coefficient over the lower half of the abutment varies linearly from K^* to the at-rest earth pressure coefficient (K_o).

$$K^* = K_o + \left(\frac{C \bullet d'}{h}\right)^{0.6} K_p \tag{3}$$

where: K_o is the at-rest earth pressure coefficient, calculated as $1 - sin\phi$ [29], h is the abutment wall height in contact with the backfill, d′ is the wall movement range $h/2$ below ground level, taken as 0.5 times the displacement range at the top of the abutment according to PD 6694–1 [12], K_p is the passive earth pressure coefficient obtained from Eurocode 7 [11] assuming an interface friction angle equal to $\phi/2$, and C is a coefficient dependent on the backfill Young's modulus (E_s) in MPa, calculated according to Eq. (4). A displacement range at the top of the abutment of 5 mm was assumed for this analysis and a value of 30 MPa was prescribed for E_s in Eq. (4).

$$C = 0.51E_S + 14.9 \quad (20 \le C \le 66) \tag{4}$$

MassDOT's [38] solution requires that the earth pressure coefficient (K_m^*) be calculated using the following empirical relationship:

$$K_m^* = 0.43 + 5.7\left[1 - e^{-190(d/h)}\right] \tag{5}$$

where d is the total displacement at the top of the abutment ($d = 5$ mm) and h is the abutment wall heigh in contact with the backfill.

The earth pressures presented a nonlinear vertical profile, with comparatively higher earth pressures toward the upper third of the abutment. The pressure magnitude increased with increasing number of cycles and tended to stabilization after cycle no. 10. The pressure distributions under annual cyclic movements diverged significantly from Rankine's passive earth pressure distribution and from those recommended by PD 6694–1 [12] and MassDOT [38]. The lateral pressures due to annual cycles significantly exceeded the distribution by PD 6694–1 [12] along the entire height after the second cycle. The lateral pressures due to annual cycles exceeded Rankine's passive condition distribution and MassDOT's [38] distribution along the abutment's upper third and above the abutment mid-height, respectively.

The resultant force corresponding to Rankine's passive condition exceeded that of the FE analysis envelope pressure distribution by almost 30 %, while the PD 6694–1 method [12] provided a resultant force with a magnitude of about one half that of the envelope pressure distribution. The resultant force from MassDOT's [38] method closely matched the distribution predicted in the FE simulation.

All design methods investigated in this analysis gave unsafe predictions of the overturning moments on the bridge abutment when compared to those predicted by the FE analysis. The shapes of the earth pressure distributions obtained with the cycles resulted in higher points of application of the resultant force, as compared to the profiles from the design methods. In Rankine's passive distribution and in MassDOT's [38] distribution, the overturning moment was placed slightly above one-third of the abutment height, while it was placed at mid-height in the distribution of PD 6649–1 [12] method. A lower point of application of the resultant force leads to a smaller overturning moment lever arm. Particularly, Rankine's passive distribution of pressures resulted in an overturning moment 23 % lower than those determined by the FE analysis.

Fig. 7 shows the evolution of the peak wall reaction ratio (K_{wp}), obtained according to Eq. (6) [20].

$$K_{wp} = \frac{P_{max}}{0.5\gamma h^2} \tag{6}$$

where: P_{max} is the maximum total soil lateral force acting on the abutment wall per unit length predicted with the FE model, γ is the unit weight of the backfill material, and h is the abutment height in contact

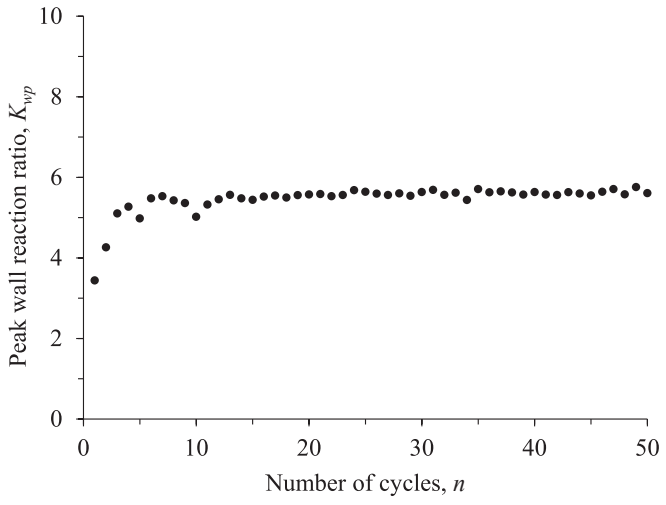

Fig. 7. Results of peak wall reaction ratios for annual cycles.

with the backfill.

It is noted that K_{wp} presents a significant nonlinear increase within the first cycles followed by stabilization. Similar results are reported elsewhere [20,52,58]. The escalation and the stabilization of the earth pressure coefficient with the cycles is a consequence of soil ratcheting, as will be discussed in following sections.

Backfill soil deformations

Fig. 8(a)-(b) present contours of accumulated compressive volumetric strains (densification) in the backfill soil after completion of cycles no. 1 and 50, respectively. Contours of expansive volumetric strains (dilation) are presented in Fig. 9(a)-(b) and cumulative deviatoric strains are shown in Fig. 10(a)-(b) for the same cycles. The data shown in Figs. 8, 9 and 10 correspond to the north abutment of the bridge. The backfill representations in Figs. 8, 9 and 10 are mirrored in relation to Fig. 2 to facilitate the use of the vertical (z/h) and horizontal (x/h) axes.

It is noted from Fig. 8 that the soil densified significantly with increasing abutment movements. Soil densification spread over a large area within the backfill, although the zone of most significant densification occurred at an abutment height ratio (z/h) around 0.7. Conversely, expansive volumetric strains occurred in a comparatively small region of the backfill near the top of the abutment and extended to a horizontal distance (x) of about 0.7 h (Fig. 9(b)).

A progressive failure involving propagation of an active shear band from the abutment toe to the soil surface developed within the backfill (Fig. 10). The shear band followed an initially curved path toward the abutment toe and reached the backfill surface at an angle to the horizontal (θ) of 60°, which corresponds to a horizontal distance (x) equal to about 0.7 h (Fig. 10(b)). The predicted angle inclination of 60° closely matched the theoretical inclination of Rankine's active failure plane. Shearing within the active shear band was also significant near the abutment top, where expansive volumetric strains occurred (Fig. 9(b)). As can be observed by comparing Fig. 10 with Figs. 8 and 9, the zone in the soil mass where most volumetric changes and shearing occurred is bounded by the active shear band.

Tatsuoka et al. [52] describes the simultaneous development of an active and a passive shear band in the soil mass as the abutment moves laterally. This mechanism, named by the authors as "dual ratchet", was confirmed experimentally [22,58,3]. A possible explanation for the absence of a passive shear band in the present study could be related to the comparatively small magnitude of the relative horizontal displacements (d/h) used in the numerical model, which is deemed insufficient to trigger the propagation of a passive shear band in the soil mass.

The accumulated deformations in the soil due to shearing and volumetric changes after each cycle resulted in significant displacements of the backfill surface. Fig. 11(a) presents profiles of the deformed backfill surface after selected annual cycles. Normalized surficial vertical displacements (s/h), obtained at the end of each cycle, are presented as a function of the normalized horizontal distance from the abutment wall (x/h). Settlements were maximum at the backfill-abutment wall interface and reduced with increasing distance from the abutment wall. The maximum settlement trough was observed to develop for cycle no. 10, after which the settlement trough reduced gradually and soil heaving initiated. The distance from the abutment wall where the backfill surface experienced large movements was approximately equal to one abutment height ($x/h = 1$) and encompassed the zone in the soil where most volumetric strains and shearing took place (Figs. 8-10).

Fig. 11(b) shows the evolution of settlements at the top of the backfill-abutment interface. It can be noted that settlements increase at a comparatively high rate during the initial five cycles and then continue to increase but at a reduced rate with increasing loading cycles. A similar trend is described by England et al. [20] and Al-Qarawi et al. [3].

Discussion

Long-term cyclic response of the backfill-abutment system

Lateral pressure variations on the abutment wall and vertical displacement variations on the backfill surface depend on the combined effects of densification and shearing that take place in the soil mass due to the cyclic lateral displacements [20]. Despite the complexity of the overall behavior of the soil mass, a simplified analysis based on the stress–strain behavior of two distinct elements of soil in the backfill is given below to provide further insight into the backfill-abutment cyclic response under the framework of the ratcheting phenomenon.

The selected elements in the backfill material, namely Element A and Element B, are located at the same height $z = 0.8\ h$ from the abutment toe, but at different distances from the abutment wall: Element A is positioned near the abutment wall, at a horizontal distance $x = 0.06\ h$, while Element B is situated at a greater distance from the wall, at $x = 0.5\ h$ (Fig. 3b). Both elements are bounded by the active shear band propagating with the cycles (Fig. 10).

Fig. 12 shows the variations of the lateral earth pressure coefficient (K), calculated according to Eq. (7), with the soil shear strain (γ_s) in the 50 annual cycles of imposed displacements on the abutment.

$$K = \frac{\sigma_h}{\sigma_{vo}} \tag{7}$$

where: σ_h is the horizontal pressure, and σ_{vo} is the initial vertical pressure prior to the cycles, at the level previously indicated.

The cyclic behavior of soil Element A resulted in positive shear strains, which are associated with compressive vertical strains and extensional horizontal strains. Conversely, Element B experienced negative shear strains, which implies extensional vertical strains and compressive horizontal strains. The evolution of the shear strains in Elements A and B was consistent with the formation of a settlement zone near the abutment wall and a heaving zone further away from the wall, as shown by the profiles of Fig. 11(a). In a granular mass, in addition to soil densification, such behavior involves the displacement of particles from the zone of settlements to the zone of heaving. This mechanism is described by England et al. [20] as "granular flow". Experimental evidence showing the downward and upward movements of particles close and far, respectively, from a wall subjected to cyclic movements can be found from the results of small-scale model tests with granular backfills reported by several researchers [52,22,3].

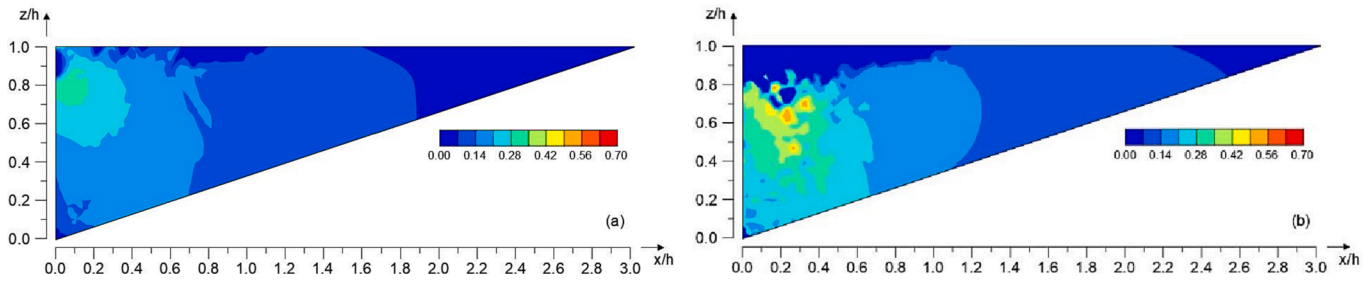

Fig. 8. Contours of cumulative compressive volumetric strains (%) in the backfill at the end of selected annual cycles: (a) cycle no. 1; (b) cycle no. 50.

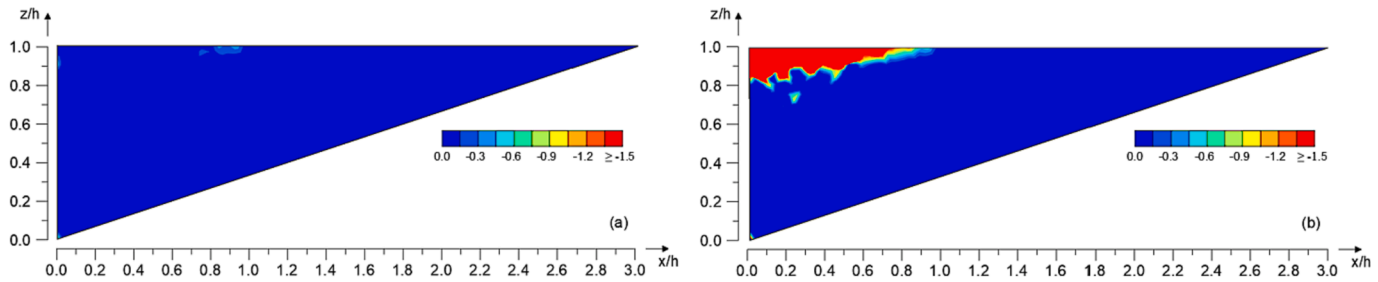

Fig. 9. Contours of cumulative expansive volumetric strains (%) in the backfill at the end of selected annual cycles: (a) cycle no. 1; (b) cycle no. 50.

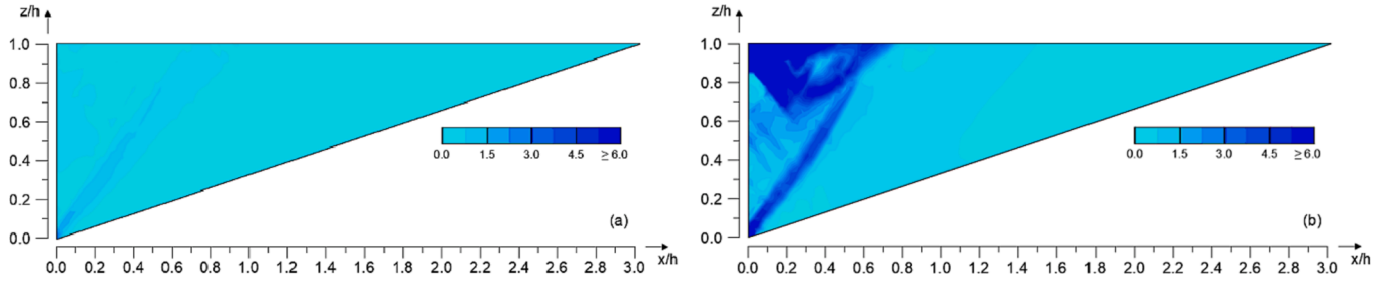

Fig. 10. Contours of accumulated deviatoric strains (%) in the backfill at the end of selected annual cycles: (a) cycle no. 1; (b) cycle no. 50.

The stress–strain behavior presented in Fig. 12 for soil Element A included open hysteresis loops during initial cycles and closed hysteresis loops after many cycles. In contrast, the response of element B involved open hysteresis loops throughout all cycles. The open hysteresis loops is associated with cumulative shear strains in the soil, while closed loops correspond to no accumulated shear strains. Open hysteresis loops are an indication that the backfill-abutment system experiences ratcheting [26].

To investigate the ratcheting phenomenon in greater depth, Fig. 13 (a) presents the cumulative shear strains ($\gamma_{s,acc}$) of Elements A and B after each cycle, obtained from the stress–strain loops shown in Fig. 12. The cumulative shear strains of Element A grew to a maximum extent with no further development beyond cycle no. 12. On the other hand, cumulative shear strains of Element B were larger than that of Element A and increased with the cycles according to a near liner fashion, without showing any tendency of levelling off. In this case, the continuous cumulative shear strains of Element B is associated with open stress–strain loops, as shown in Fig. 12. In other words, ratcheting due to shear strains takes place in the soil at greater distances from the abutment wall.

Fig. 13(b) illustrates the evolution of the cumulative volumetric strains ($\varepsilon_{v,acc}$) in Elements A and B. Soil densification (i.e., positive volumetric strains) was observed with both investigated elements and increased with the proximity to the abutment wall. The cumulative volumetric strain escalation of Element A was rapid during the first three cycles and then reduced considerably until cycle no. 15, when it reached a steady state. On the other hand, cumulative volumetric strain changes of Element B were nearly zero during the 50 cycles of movement of the bridge abutment.

In summary, the simulations showed that, during the abutment cyclic movements, cumulative shear strains prevailed in the region of the backfill soil far from the abutment wall, while cumulative compressive volumetric strains (densification) dominated in the zone adjacent to the soil-abutment interface. While densification increased soil stiffness and consequently the lateral pressure on the abutment wall, shear strains in the soil away from the wall contributed to alleviate the lateral pressures on the wall. Ultimately, a balance between both effects was reached, resulting in the stabilization of the peak wall reaction ratio, K_{wp} (Fig. 7). Justification for settlements at the soil-abutment interface continuing to persist while K_{wp} stabilized, as shown in Fig. 11(b), was due to the continued growth of the cumulative shear strains at a distance from the abutment wall (Fig. 13(a)).

Practical implications

The numerical analyses conducted as part of this investigation revealed that the horizontal cyclic movements of the semi-integral bridge abutment lead to a rapid escalation of lateral pressures on the wall during the initial few years of operation of the bridge. Two methods developed specifically for predicting the lateral pressures behind the abutment of integral bridges were assessed: the method proposed by the Massachusetts Department of Transportation [38] and the solution proposed in PD 6649–1 [12]. The pressure distribution obtained according to Rankine's passive condition was also evaluated for comparisons, since several design guidelines propose using passive pressure distributions behind integral abutments [4].

The analysis of the outcome of these solutions revealed that a design approach using the method proposed in guideline PD 6649–1 [12] would be unconservative for the studied abutment because it provides lateral soil pressures of excessively low magnitudes along the abutment height. Conversely, a design approach based on Rankine's passive pressure distribution would overestimate the lateral force magnitudes on the wall. Additionally, care should be exercised when applying these two methods because both are likely to underestimate the long-term growing of the overturning moments on the abutment upon cycling. Although a design approach using MassDOT's [38] method could result in good predictions of the long-term lateral force on the abutment wall, it would likely result in unconservative overturning moment predictions. In view of this, analytical methods incorporating pressure distributions with higher lateral pressures at the upper third of the abutment and lower lateral pressures below that level, should be pursued.

The performed numerical simulations revealed that the annual cyclic movements of the bridge abutment result in both settlements near the soil-wall interface and heaving at a distance from the wall. Results presented in Fig. 11(a) suggest that the differential settlement between the abutment and the backfill surface is enough to lead the approach road asphalt to cracking at the road-bridge deck interface, which can be detrimental to the bridge performance. Accordingly, a field inspection

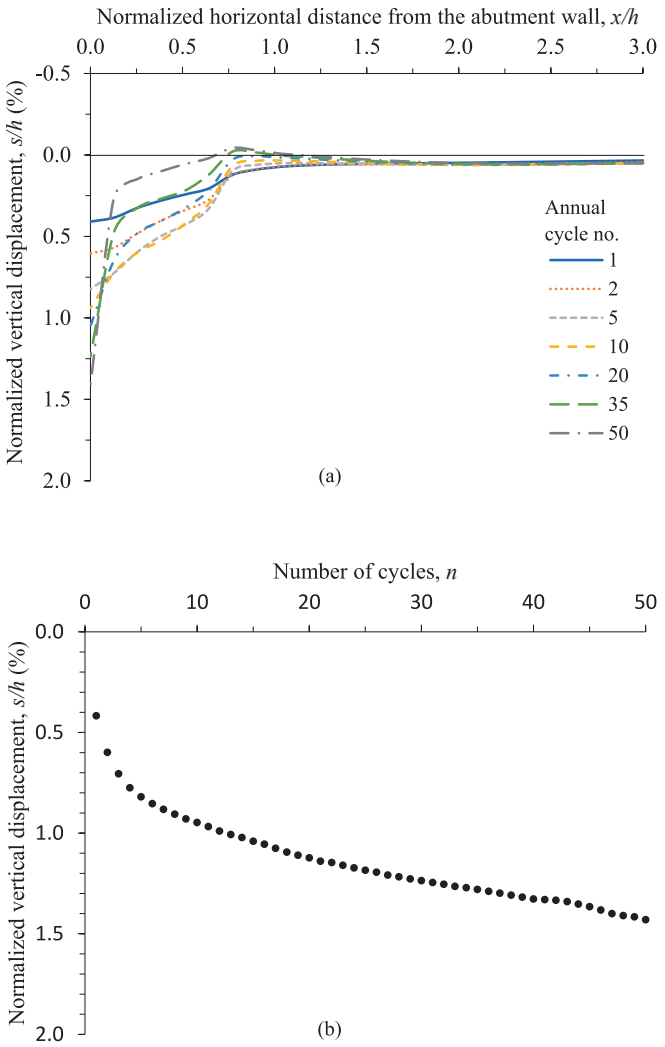

Fig. 11. (a) Vertical displacement profiles of the backfill surface for selected annual cycles; (b) normalized vertical displacement at backfill-abutment interface *versus* number of annual cycles.

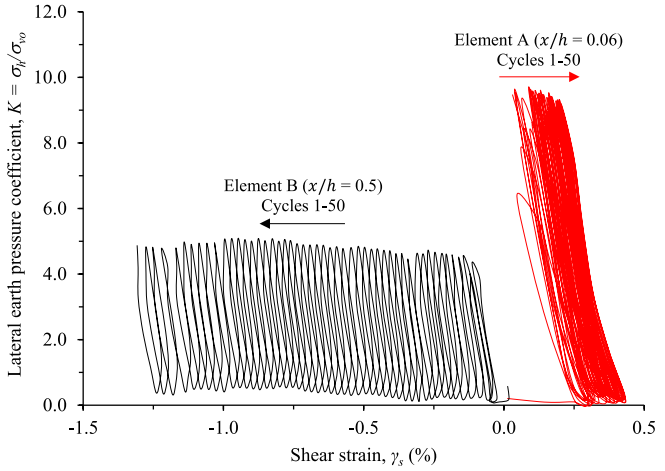

Fig. 12. Earth pressure coefficient variation for Elements A and B over 50 annual cycles.

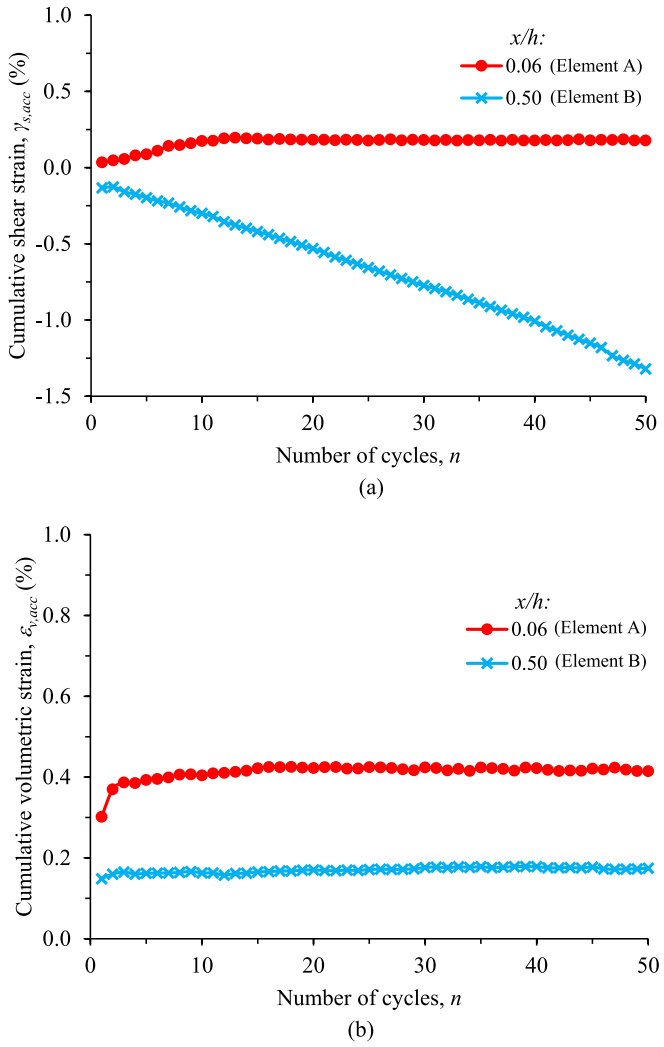

Fig. 13. (a) Cumulative shear strain changes with the cycles; (b) Cumulative compressive volumetric strain changes with the cycles.

conducted 270 days after construction completion visually confirmed a depression between the approach road and the bridge deck in both north and south bridge abutments [59]. Although other construction issues may have also affected the bridge performance, the semi-integral nature of the structure may be attributed to such excessive settlements of the backfill.

The vertical displacements of the backfill surface were significantly influenced by the cyclic lateral movements of the abutment within a distance equivalent to about one abutment height (1 *h*) from the abutment wall (Fig. 11(a)). Therefore, solutions to reduce the evolution of the vertical displacements should be implemented along a distance equal to one abutment height from the abutment-soil interface, at minimum. Available solutions to alleviate approach problems include reinforcing the backfill with geogrid layers [52], backfilling with tire-derived aggregate-soil mixtures [5], reinforcing the backfill with geocell layers [58], and using expanded polystyrene geofoam inclusions [3].

Concluding remarks

This paper presented results of a two-dimensional FE investigation on the interaction between a semi-integral concrete bridge abutment and a granular backfill under cyclic lateral movements of the abutment. The numerical model was validated by comparing predicted results against field data from pressure cells installed behind the abutment of a

semi-integral bridge located near the City of Palestine, Texas, USA. The response of the backfill-abutment system was assessed for annual thermal amplitudes within a 50-year period. Emphasis was placed on examining both lateral earth pressures on the abutment and deformations in the backfill soil with the cycles. The results of the numerical analysis obtained herein indicate that:

(1) Annual cyclic lateral movements of the bridge abutment led to a rapid increase of lateral earth pressures behind the abutment wall. The locus of maximum lateral earth pressures was predicted to occur in the upper third of the abutment, which is inconsistent with typical earth pressure distributions assumed in design guidelines for integral bridge abutments. However, the pressure distribution proposed in the LRFD Bridge Design Guidelines of the Massachusetts DOT [38] showed good agreement with the lateral pressures obtained on the abutment wall for a range of cyclic movements representing a 50-year return period. In contrast, the pressure distributions due to guideline PD 6649–1 [12] and Rankine's passive earth pressure condition provided comparatively low and high lateral forces on the abutment wall, respectively, as compared to the pressure distributions obtained with the same annual movement range.
(2) Progressive failure of the backfill soil predicted under annual cycles involved propagation of an active shear band from the abutment toe, which intersected the backfill surface at an inclination consistent with Rankine's active failure surface. Strains due to shearing and volumetric changes in the backfill soil were predicted to accumulate during the cyclic loading, implying the development of soil ratcheting. Manifestation of cumulative shear strains and cumulative compressive volumetric strains (densification) in the soil mass was particularly intense in the backfill zone bounded by the active shear band and abutment wall face.
(3) The straining within the backfill soil resulted in a settlement trough near the backfill-abutment interface and heaving at greater distances. The largest vertical displacements of the backfill surface took place within a horizontal distance from the abutment wall of approximately-one abutment height. The magnitude of the settlement trough predicted to develop with the annual cycles is deemed sufficient to negatively impact the bridge performance soon after the start of the bridge operation.
(4) Based on the numerical simulations, cumulative shear strains prevailed in the region of the backfill soil far from the abutment wall, while cumulative compressive volumetric strains (densification) dominated in the zone adjacent to the soil-abutment interface. The continued growth of cumulative shear strains denotes the occurrence of ratcheting. While densification increased soil stiffness and consequently the lateral pressure on the abutment wall, cumulative shear strains in the soil away from the wall contributed to alleviation of lateral earth pressures. A balance between both effects resulted in stabilization of lateral earth pressures on the soil-abutment interface with the cycles. Conversely, settlements adjacent to the soil-abutment interface persisted with the annual cycles, because of continued growth of cumulative shear strains in the portion of the soil away from the abutment wall.

CRediT authorship contribution statement

Pedro H.S. Silva: Data curation, Formal analysis, Investigation, Writing – original draft, Methodology, Validation, Visualization. **Yuri D. J. Costa:** Conceptualization, Formal analysis, Methodology, Resources, Supervision, Writing – review & editing. **Jakob R. Walter:** Investigation, Writing – review & editing. **Behdad M. Kouchaki:** Investigation, Validation. **Jorge G. Zornberg:** Conceptualization, Resources, Supervision, Writing – review & editing. **Carina M.L. Costa:** Supervision, Writing – review & editing.

Declaration of Competing Interest

The authors declare that they have no known competing financial interests or personal relationships that could have appeared to influence the work reported in this paper.

Data availability

Data will be made available on request.

Acknowledgements

This research was sponsored by the National Council for Scientific and Technological Development (CNPq), Brazil (Grant No. 429217/2018-8) and by the Texas Department of Transportation (TxDOT) (Proj. 0-6936). The financial support is gratefully acknowledged.

References

[1] Aashto. LRFD bridge design specifications. 8th ed. New York: AASHTO; 2017.
[2] Abdel-Fattah MT, Abdel-Fattah TT. Behavior of integral frame abutment bridges due to cyclic thermal loading: nonlinear finite-element analysis. J Bridge Eng 2019; 24(5):04019031. https://doi.org/10.1061/(ASCE)BE.1943-5592.0001394.
[3] Al-Qarawi A, Leo C, Liyanapathirana DS. Effects of wall movements on performance of integral abutment bridges. Int J Geomech 2020;20(2):04019157. https://doi.org/10.1061/(ASCE)GM.1943-5622.0001559.
[4] Arenas AE, Filz GM, Cousins TE. Thermal response of integral abutment bridges with mechanically stabilized earth walls. Blacksburg (VA): Virginia Polytechnic Institute & State University; 2013. Report No.: VCTIR 13-R7. Sponsored by Virginia Department of Transportation.
[5] Argyroudis S, Palaiochorinou A, Mitoulis S, Pitilakis D. Use of rubberized backfills for improving the seismic response of integral abutment bridges. Bull Earthq Eng 2016;14:3573–90. https://doi.org/10.1007/s10518-016-0018-1.
[6] Arsoy S, Duncan JM, Barker RM. Behavior of a semiintegral bridge abutment under static and temperature-induced cyclic loading. J Bridge Eng 2004;9(2):193–9. https://doi.org/10.1061/(ASCE)1084-0702(2004)9:2(193).
[7] Banks JR, Bloodworth AG. Lateral stress profiles on integral bridge abutments. Proc Inst Civ Eng –. Bridge Eng 2018;171(3):155–68. https://doi.org/10.1680/jbren.17.00017.
[8] Bloodworth AG, Xu M, Banks JR, Clayton CRI. Predicting the earth pressure on integral bridge abutments. J Bridge Eng 2012;17(2):371–81. https://doi.org/10.1061/(ASCE)BE.1943-5592.0000263.
[9] Breña SF, Bonczar CH, Civjan SA, Dejong JT, Crovo DS. Evaluation of seasonal and yearly behavior of an integral abutment bridge. J Bridge Eng 2007;12(3):296–305. https://doi.org/10.1061/(ASCE)1084-0702(2007)12:3(296).
[10] Brinkgreve RBJ, Kumarswamy S, Swolfs WM. Plaxis 2D version 2016: reference manual. Delft: Plaxis bv; 2016.
[11] BSI. BS EN 1997-1:2004+A1:2013. NA to Eurocode 7: Geotechnical design – Part 1: general rules. London; 2014.
[12] Bsi. PD 6694–1: 2011. Recommendation for the design of structures subject to traffic loadings to BS EN 1997–1: 2004. London: BSI; 2011.
[13] Burke Jr MP. Integral & semi-integral bridges. 1st ed. Oxford: Wiley & Sons; 2009.
[14] Caristo A, Barnes J, Mitoulis SA. Numerical modelling of integral abutment bridges under seasonal thermal cycles. Proc Inst Civ Eng –. Bridge Eng 2018;171(3): 179–90. https://doi.org/10.1680/jbren.17.00025.
[15] Civjan SA, Bonczar C, Brena SF, DeJong J, Crovo D. Integral abutment bridge behavior: parametric analysis of a Massachusetts bridge. J Bridge Eng 2007;12(1): 64–71. https://doi.org/10.1061/(ASCE)1084-0702(2007)12:1(64).
[16] Civjan SA, Kalayci E, Quinn BH, Brena SF, Allen CA. Observed integral abutment bridge substructure response. Eng Struct 2013;56:1177–91. https://doi.org/10.1016/j.engstruct.2013.06.029.
[18] Duncan JM, Chang C. Nonlinear analysis of stress and strain in soils. J Soil Mech Found Div 1970;96(5):1629–53.
[19] Emerson M. Temperature differences in bridges: basis of design requirements. Crowthorne (Berks): Transport and Road Research Laboratory; 1977. Report No.: 765.
[20] England GL, Tsang NCM, Bush DI. Integral bridges: a fundamental approach to the time-temperature loading problem. 1st ed. London: Thomas Telford; 2000.
[21] Frosch RJ, Lovell MD. Long-term behavior of integral abutment bridges. West Lafayette (IN): Purdue University; 2011. Report No.: FHWA/IN/JTRP-2011/16. Contract No.: SPR-3223. Sponsored by Indiana Department of Transportation.
[22] Gabrieli F, Zorzi G, Wan R. Granular ratcheting phenomena behind a model retaining wall. In: Soga K, Kumar K, Biscontin G, Kuo M, editors. Geomechanics from micro to macro. London: Taylor & Francis Group; 2015. p. 601–6.
[23] Geokon. Instruction manual: model 4800 series VW earth pressure cells. Lebanon: Geokon; 2019.
[24] Gerdau. Steel sheet piling: quick reference guide. Midlothian: Gerdau; 2019.

[25] Hamoudi MM, Coyle HM, Bartoskewitz RE. Correlation of the Texas Highway Department Cone Penetrometer test with unconsolidated-undrained shear strength of cohesive soils. College Station (TX): Texas Transportation Institute; 1974. Report No.: Research Report 10–1. Contract No.: Research Studv 2-5-74-10. Sponsored by Texas Highway Department.
[26] Houlsby GT, Abadie CN, Beuckelaers WJAP, Byrne BW. A model for nonlinear hysteretic and ratcheting behaviour. Int J Solids Struct 2017;10:42. https://doi.org/10.1016/j.ijsolstr.2017.04.031.
[27] Huntley SA, Valsangkar AJ. Field monitoring of earth pressures on integral bridge abutments. Can Geotech J 2013;50:841–57. https://doi.org/10.1139/cgj-2012-0440.
[28] Imbsen RA, Vandershaf DE, Schamber RA, Nutt RV. Thermal effects in concrete bridge superstructures. New York (NY): Transportation Research Board; 1985. Report No.: 276.
[29] Jaky J. The coefficient of earth pressure at rest. [In Hungarian] J Soc Hung Eng Arch 1944:355–8.
[30] Janbu N. Soil compressibility as determined by oedometer and triaxial tests. In: Problems of Settlements and Compressibility of Soils. Proceeding of European Conference on Soil Mechanics and Foundation Engineering; 1963; Wiesbaden, Germany. Wiesbaden: ISSMFE; 1963. p. 19-25.
[31] Karalar M, Dicleli M. Fatigue in jointless bridge H-piles under axial load and thermal movements. J Constr Steel Res 2018;147:504–22. https://doi.org/10.1016/j.jcsr.2018.05.006.
[32] Kim W, Laman JA. Seven-year field monitoring of four integral abutment bridges. J Perform Constr Facil 2012;26(1):54–64. https://doi.org/10.1061/(ASCE)CF.1943-5509.0000250.
[33] Knappett JA, Caucis K, Brown MJ, Jeffrey JR, Ball JD. CHD pile performance: part II – numerical modelling. Proc Inst Civ Engineers –. Geotech Eng 2016;169(5):436–54. https://doi.org/10.1680/jgeen.15.00132.
[34] Kulhawy FH, Mayne PW. Manual on estimating soil properties for foundation design. New York (NY): Cornell University; 1990. Report No.: 1493-6. Contract No.: EL-6800. Sponsored by Eletric Power Research Institute.
[35] Lee DJ. Bridge bearings and expansion joints. 2 ed. London: E & FN Spon; 1994.
[36] Mahendran M. In: The modulus of elasticity of steel: is it 200 GPa? St. Louis, USA. St. Louis: Missouri University of Science and Technology; 1996. p. 641–8.
[37] Maruri RF, Petro SH. In: Integral abutments and jointless bridges (IAJB) 2004 survey summary. Maryland, USA. Maryland: FHWA; 2005. p. 12–29.
[38] MassDOT LRFD. bridge design guidelines. Boston: MassDOT; 2020.
[39] Mesri G. Discussion on "New design procedure for stability of soft clays". J Geotech Eng Div 1975;101:409–12.
[40] Mitoulis SA, Palaiochorinou A, Georgiadis I, Argyroudis S. Extending the application of integral frame abutment bridges in earthquake-prone areas by using novel isolators of recycled materials. Earthq Eng Struct Dyn 2016;45:2283–301. https://doi.org/10.1002/eqe.2760.
[41] Muszynski Z, Wyjadlowski M. Assessment of the shear strength of pile-to-soil interfaces based on pile surface topography using laser scanning. Sens 2019;19(5):1–21. https://doi.org/10.3390/s19051012.
[42] Naval Facility EngineeringCommand NFE. Foundation and earth structures. Alexandria: Naval Facilities Engineering Command; 1986.
[43] Obrzud RF, Truty A. The hardening soil model – a practical guidebook. Preverenges: Zace Services Ltd; 2018.
[44] Peric D, Miletic M, Shah BR, Esmaeily A, Wang H. Thermally induced soil structure interaction in the existing integral bridge. Eng Struct 2016;106:484–94. https://doi.org/10.1016/j.engstruct.2015.10.032.
[45] Rankine W. On the stability of loose earth. Philos Trans Royal Soc Lond 1857;147.
[46] Rawat S, Gupta AK. Numerical modelling of pullout of helical soil nail. J Rock Mech Geotech Eng 2017;9(4):648–58. https://doi.org/10.1016/j.jrmge.2017.01.007.
[47] Salkind NJ. Statistics for people who (think they) hate statistics. 6 ed. Thousand Oaks: SAGE; 2017.
[48] Schanz T, Vermeer PA. Special issue on pre-failure deformation behaviour of geomaterials. Géotech 1998;48:383–7.
[49] Schanz T, Vermeer P, Bonier P. Formulation and verification of the Hardening Soil model. Rotterdam: Balkema; 1999.
[50] Stroud MA, Butler FG. The standard penetration test and the engineering properties of glacial materials. In: Midland Soil Mechanics and Foundation Engineering Society, editors. The Engineering Behaviour of Glacial Materials. Proceedings of the Symposium on Engineering Properties of Glacial Materials; 1975 Apr 21-23; Birmingham, USA. Birmingham: Midland Geotech. Society; 1975. p. 124-135.
[51] Suchsland O, Woodson GE. Fiberboard manufacturing practices in the United States. Washington: Department of Agriculture; 1987.
[52] Tatsuoka F, Hirakawa D, Nojiri M, Aizawa H, Nishikiori H, Soma R, et al. A new type of integral bridge comprising geosynthetic-reinforced soil walls. Geosynth Int 2009;16(4):301–29. https://doi.org/10.1680/gein.2009.16.4.301.
[53] Tomlinson MJ. Pile design and construction practice. London: E & FN Spon; 1993.
[54] TxDOT. Geotechnical manual. Austin: TxDOT; 2020.
[55] TxDOT. Designation Tex-132-E: test procedure for Texas Cone Penetration. Austin: TxDOT; 1999.
[56] Vipulanandan C, Puppala AJ, Jao M, Kim MS, Vasudevan H, Kumar P, et al. Correlation of Texas Cone Penetrometer test values and shear strength of Texas soils. Houston (TX): University of Houston; 2008. Report No.: FHWA/TX-08/0-4862-1. Contract No.: 0-4862. Sponsored by Texas Department of Transportation.
[57] Walter JR. Experimental and numerical investigation of integral/semi-integral bridge abutments for Texas conditions [thesis]. Austin (TX): The University of Texas at Austin; 2018.
[58] Zadehmohamad M, Bazaz JB. Cyclic behaviour of geocell-reinforced backfill behind integral bridge abutment. Int J Geotech Eng 2019;13(5):438–50. https://doi.org/10.1080/19386362.2017.1364882.
[59] Zornberg JG, Mofarraj B, Costa Y, Silva P, Helwig T. TxDOT project 0-6936: development of integral/semi-integral abutments for Texas bridges. Austin (TX): The University of Texas at Austin; 2019. Report No.: FY'19 TMB. Sponsored by Texas Department of Transportation.
[60] Zorzi G, Artoni R, Gabrieli F. Experiments and DEM simulations of granular ratcheting. In: Radjai F, Nezamabadi S, Luding S, Delenne JY, editors. Powders and Grains 2017. Proceedings of the 8th International Conference on Micromechanics on Granular Media; 2017 Jul 3-7; Montpellier, France. EPJ Web Conferences; 2017. 03061. 10.1051/epjconf/201714003061.

Further reading

[17] Duderstadt FJ, Coyle HM, Bartoskewitz RE. Correlation of the Texas Cone Penetrometer test N-value with soil shear strength. College Station (TX): Texas A&M University; 1977. Report No.: FHWATX77-10-3F. Contract No.: Research Study 2-5-74-10. Sponsored by Texas State Department of Highways and Public Transportation.